Materials Letters 185 (2016) 197–200

Contents lists available at ScienceDirect

Materials Letters

journal homepage: www.elsevier.com/locate/matlet

Facile microwave-assisted hydrothermal synthesis of hexagonal sodium tungsten bronze and its high response to NO_2

Tiago A. Martins [a], Thales R. Machado [a,b], Mateus M. Ferrer [a], Sonia M. Zanetti [c,*], Elson Longo [c]

[a] INCTMN-UFSCar, São Carlos, São Paulo, 13565-905 Brazil
[b] DQIO, Universitat Jaume I, Castellón, 12071 Spain
[c] INCTMN-UNESP, Araraquara, São Paulo, 14801-907 Brazil

ARTICLE INFO

Article history:
Received 21 June 2016
Received in revised form
25 August 2016
Accepted 27 August 2016
Available online 27 August 2016

Keywords:
Microwave-assisted hydrothermal method
Gas sensor
Sodium tungsten bronze
Nanoplates

ABSTRACT

Single-phase hexagonal sodium tungsten bronze (h-$Na_xWO_{3+x/2}\cdot yH_2O$) was synthesized via a microwave-assisted hydrothermal method. A reaction time of 4 min was sufficient to obtain well-crystallized nanoplates with a thickness of 5–16 nm and length of 5–500 nm. The structure, morphology, and composition of the obtained material were characterized by X-ray diffraction and scanning electron microscopy. H_2O molecules and Na species were detected in the hexagonal channels of the tungsten bronze structure. The gas sensing properties were also measured, suggesting that h-$Na_xWO_{3+x/2}\cdot yH_2O$ can be a promising material for NO_2 detection due to the high response observed.

1. Introduction

Tungsten bronze structures (M_xWO_3, where M represents species in the interstitial sites of a modified WO_3 matrix) have attracted increasing attention because of their ferroelectricity, superconductivity, and potential applications including solar filters, smart windows, and humidity sensors [1–4]. However, the gas sensing properties associated to tungsten bronze structures have rarely been reported. Among other metal oxides, such as SnO_2, TiO_2, ZnO, and In_2O_3, hexagonal WO_3 is a well-known gas sensor with high sensitivity, selectivity, enhanced response, and recovery time [5]. Tungsten bronze structures could be potentially used for this application because of the structural similarities with WO_3. Both materials are formed by octahedral WO_6 arrays, which originate hexagonal channels. For M_xWO_3, the hexagonal channels are filled with M species, including alkali metals (Cs, Li, K, and Na) and some small molecules, such as water or ammonium [2,3].

Moreover, these species play an important role on the final properties of the prepared materials because the presence of Na in h-$Na_xWO_{3+x/2}\cdot yH_2O$ induces the formation of trap centers, improving the photocatalytic activity. The cation also modifies the number of adsorption sites of h-$Na_xWO_{3+x/2}\cdot yH_2O$, which can lead to an improved response of the gas sensor.

Different strategies have been reported to prepare tungsten bronze structures, such as hydrothermal processes [3], solid-state reactions [6], and sol-gel methods [7]. High temperatures and/or long periods are generally necessary to synthesize single-phase tungsten bronzes [3,6].

In this study, we report the synthesis of h-$Na_xWO_{3+x/2}\cdot yH_2O$ using a microwave-assisted hydrothermal method, which is cost-effective due to its fast kinetic process [8]. We also demonstrate that h-$Na_xWO_{3+x/2}\cdot yH_2O$ can act as a NO_2 sensor, with the advantages of potential selectivity, facile synthesis, and high sensibility at concentrations that affect the human health [9–11].

2. Experimental procedure

The following procedure was used to synthesize the h-$Na_xWO_{3+x/2}\cdot yH_2O$ powder. Firstly, 2 g of $Na_2WO_4\cdot 2H_2O$ (99%, Sigma-Aldrich) was dissolved in 45 mL of distilled water under stirring at room temperature for 5 min. Then, 5 mL of a 3 M HCl solution was added under continuous stirring for an additional 5 min. The yellowish product was placed in a closed Teflon reaction cell and heated using a conventional microwave furnace (2.5 GHz, 800 W) at 150 °C for 4 min. The resulting precipitate was washed several times with distilled water, and dried at 80 °C for 12 h under air atmosphere (MH sample). The resulting powder was heat-treated at 300 °C for 2 h with a heating rate of 5 °C min^{-1} to eliminate volatiles (MH300C sample).

* Corresponding author.
E-mail address: zanetti@iq.unesp.br (S.M. Zanetti).

http://dx.doi.org/10.1016/j.matlet.2016.08.126
0167-577X/

The samples were characterized by X-ray diffraction (XRD, Rigaku D/Max-2500 V/PC, Cu-Kα radiation), Raman spectroscopy (iHR550 micro-Raman spectrometer, Horiba Jobin-Yvon, Japan) coupled with a CCD detector operating with an Ar-ion laser (Melles Griot, USA), Fourier transform infrared spectroscopy (FTIR, Bruker, Equinox 55), UV–Vis absorption (Varian Cary 5 G), field emission scanning electron microscopy (FE-SEM, Zeiss Supra 35), and energy dispersive X-ray spectroscopy (EDX, LEO, model 440, Leica).

The sensor devices were fabricated on alumina substrates with interdigitated pre-printed Ag-Pd electrodes on the top and a Ag-Pd heating resistor on the bottom to control the working temperature during the measurements. The sensor elements were prepared by mixing 10 mg of h-$Na_xWO_{3+x/2}\cdot yH_2O$ powder with 5 μL of α-terpineol in a mortar to obtain a slurry that was coated on the substrate. The thick film was dried at 60 °C, followed by heating at 300 °C for 2 h to remove organics.

The sensing tests were carried out in a 220 mL-glass chamber under gas flow. Synthetic air was used as both carrier and purging gas at a constant flow rate of 100 cm^3 min^{-1}, and 100 ppm of NO_2 in air was used as analyte gas. The desired NO_2 concentrations were obtained using calibrated mass-flow controllers.

The sensor resistance was measured continuously using a Keithley 6437 picoammeter (bias voltage of 1 V). Synthetic air flowed through the chamber during heating (working temperature of 200 °C), and then the specific NO_2 concentration flowed during 10 min. Finally, the NO_2 flow was removed, and the chamber was purged with synthetic air during 20 min for cleaning. This procedure was repeated for each NO_2 concentration (10–80 ppm). The sensor response was calculated using $S=R_g/R_a$, where R_g and R_a are the resistances in NO_2 and in air flow, respectively. The response and recovery times were defined as the time required by the sensor to reach 90% of the total resistance variation in the case of adsorption and desorption, respectively.

3. Results and discussion

Fig. 1(a) shows the XRD patterns of the MH and MH300C samples. All peaks were indexed to pure h-$Na_xWO_{3+x/2}\cdot yH_2O$ with a *P6/mmm* space group (Inorganic Crystal Structure Data No. 071931). Both MH and MH300C samples show narrow and intense diffraction peaks with a crystallite size of 22 and 15 nm, respectively. The crystallite size decrease after the heat treatment might be related to the loss of structural water at around 300 °C, which is common for hydrated tungsten oxides [12].

The FTIR and Raman bands shown in Fig. 1(b) and Fig. 1(c) are summarized in Table 1. The detected bands are in good agreement with previous studies. Specifically, the bands at 3604 and 3545 cm^{-1} of the FTIR spectra, and the bands at 320 and 948 cm^{-1}

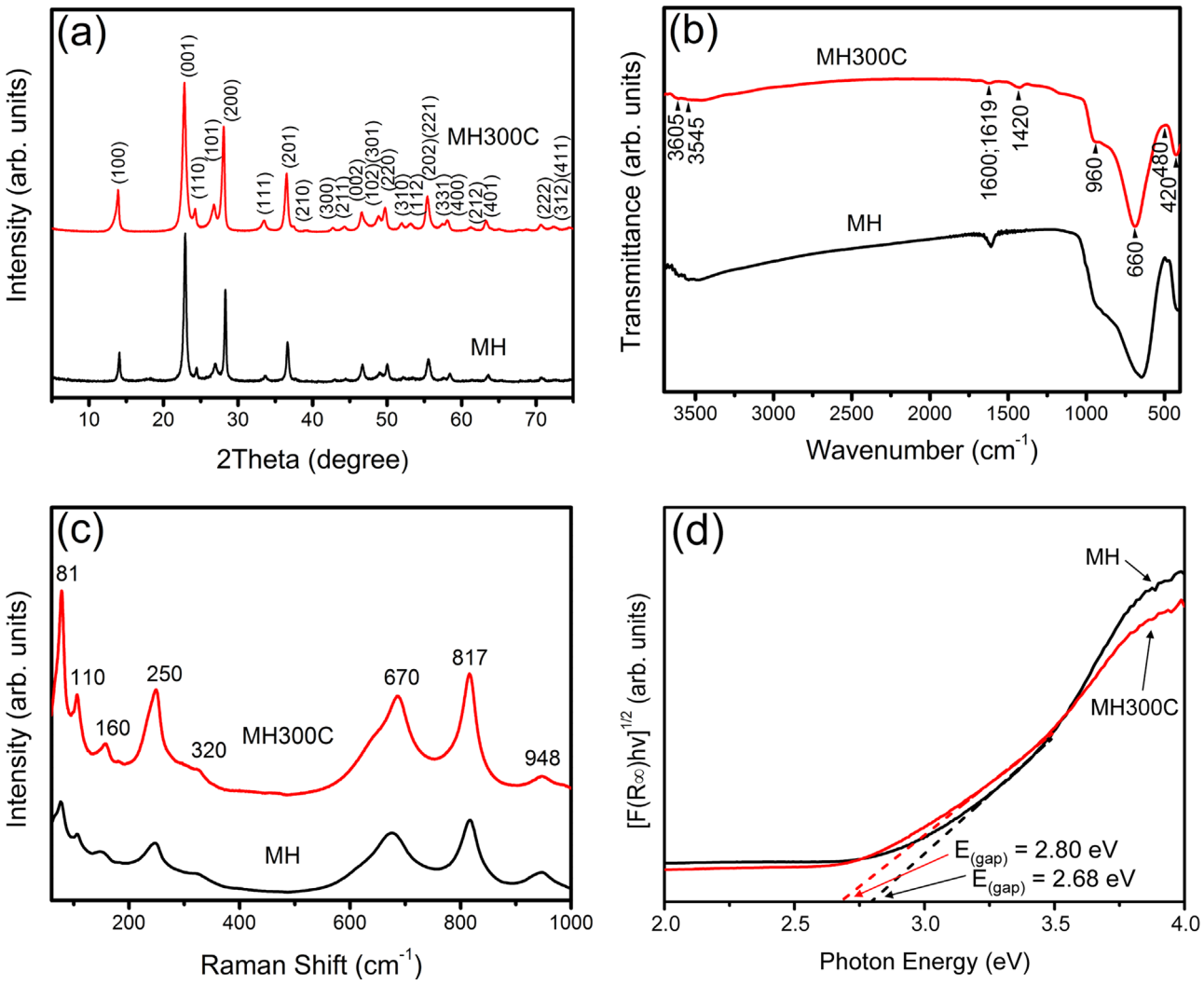

Fig. 1. (a) XRD patterns, (b) FTIR spectra, (c) Raman spectra, and (d) UV–Vis absorption spectra for the MH and MH300C samples.

Table 1
Vibrational properties of $Na_xWO_{3+x/2} \cdot yH_2O$.

Vibrations	FTIR band (cm^{-1})	Reference	Vibrations	Raman band (cm^{-1})	Reference
υ(W–OH_2)	420	[3,19]	Lattice modes	81	[19]
δ(O–W–O)	480	[3]		110	[19]
υ(O–W–O)	660	[13–19]		160	[19]
υ(O=W)	960	[3,19]	δ(O–W–O)	250	[19]
δ(OH)	1410	[13–19]	υ(W–OH_2)	320	[19]
δ(H_2O)	1600	[3,13]	υ(O–W–O)	670	[19]
δ(OH)	1619	[3,19]	υ(O–W–O)	817	[19]
υ(H_2O)	3545	[3,13]	υ(W=O)	948	[13,19]
υ(H_2O)	3605	[3]			

υ for stretching vibration, and δ for bending vibration.

of the Raman spectra confirm the presence of structural water in the hexagonal channels. The presence of water and Na in the hexagonal channels can modify the number of adsorption sites of h-$Na_xWO_{3+x/2} \cdot yH_2O$, besides interacting with the electrons (e−) and holes (h+) produced in the semiconductor, improving their electronic properties compared to WO_3 [3].

The band-gap energy ($E_{(gap)}$) is related to the chemical composition of h-$Na_xWO_{3+x/2} \cdot yH_2O$, where x=0.17–0.25. If the value of x is greater than 0.25, the material exhibits a metallic character with a very small $E_{(gap)}$ value, and the formation of tetragonal or cubic phases [3,15].

Fig. 1(d) shows the UV–Vis spectra of the MH and MH300C samples; the optical band-gaps were 2.8 and 2.7 eV, respectively, using the Kubelka-Munk method [16]. These high $E_{(gap)}$ values are very similar to those of WO_3, which vary from 2.6 to 3.25 [17,18], confirming the formation of a hexagonal phase with a semiconductor character, which is fundamental to the sensing properties.

Fig. 2(a) and Fig. 2(b) show FE-SEM micrographs of the MH and MH300C samples, respectively. They are composed of irregular nanoplates with a thickness of 5–16 nm and length of 5–500 nm. This particle shape is commonly observed for $WO_3 \cdot xH_2O$ and WO_3 materials, obtained by acidification and using $Na_2WO_4 \cdot 2H_2O$ as precursor [20]. The elemental analysis carried out using EDX (Fig. 2(c)) indicated the presence of W (29.7 at%), Na (2.37 at%), and O (67.9 at%) for the MH300C sample, corroborating the XRD, Raman, and FTIR results.

The MH300C sample was exposed to a NO_2 flow of 10, 20, 40, and 80 ppm (Fig. 3) at a working temperature of 200 °C. The sensor responses observed for these NO_2 concentrations were 18, 115, 204, and 233, respectively; these are higher or similar to those of WO_3-based sensors (90 and 22 at 80 ppm and 10 ppm, respectively) at 250 °C [21,22]. Moreover, a fast response time of ~3 min, and a recovery time of ~12 min were obtained for all samples. The sensor did not exhibit a good response to CO, CH_4, and H_2, showing a potential selectivity to NO_2. These results demonstrate the viability of the obtained h-$Na_xWO_{3+x/2} \cdot yH_2O$ structure for gas sensing applications.

We propose a sensing mechanism based on a cluster-to-cluster charge transfer, from a cluster with Na ions to a cluster with a neutral vacancy, as shown in the following reactions:

$$[WO_5V_o^{x}Na] + [WO_6]^{x} \rightarrow [WO_5V_o^{\bullet}Na] + [WO_6]' \quad (1)$$

$$[WO_5V_o^{\bullet}Na] \bullet\bullet\bullet NO_2 \rightarrow [WO_5V_o^{\bullet}Na]\ \bullet\bullet\bullet NO_2 \quad (2)$$

$$2[WO_5V_o^{\bullet}Na] \bullet\bullet\bullet NO_2 \rightarrow 2[WO_5V_o^{\bullet}Na]\ \bullet\bullet\bullet NO^{*} + O_2 \quad (3)$$

$$2[WO_5V_o^{\bullet}Na]\ \bullet\bullet\bullet NO^{*} + O_2 \rightarrow 2[WO_5V_o^{\bullet}Na] + 2NO_2 \quad (4)$$

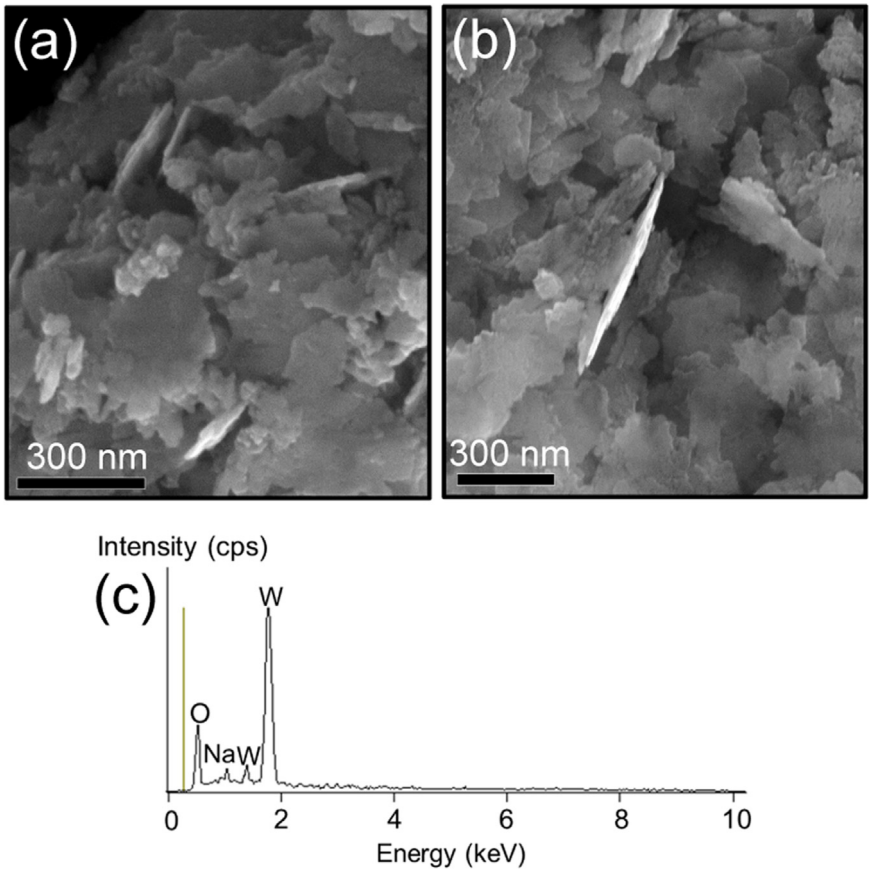

Fig. 2. FE-SEM micrographs of (a) MH, and (b) MH300C samples; (c) EDX analysis of MH300C.

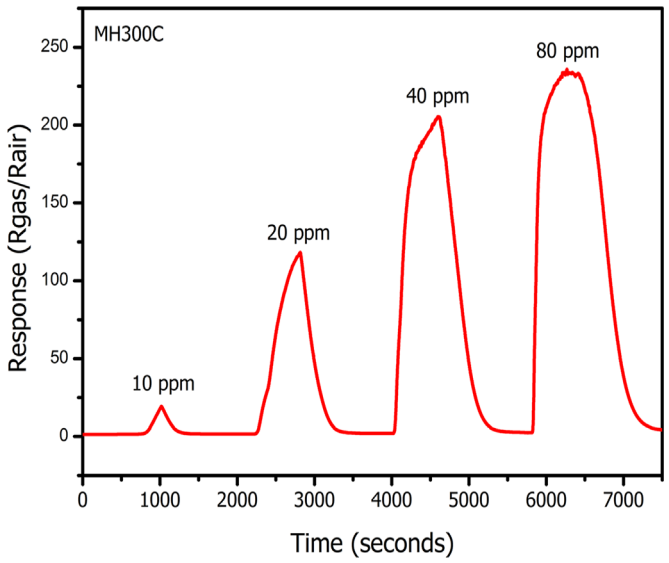

Fig. 3. Response of the h-$Na_xWO_{3+x/2} \cdot yH_2O$ nanoplates to NO_2 at 200 °C.

NO_2 is adsorbed on a positive vacancy (Eq. (2)) and is subsequently dissociated (Eq. (3)) with the release of O_2. After stopping the NO_2 flow, the remaining NO* molecule interacts with oxygen from air, releasing NO_2 again (Eq. (4)).

4. Conclusions

In summary, h-$Na_xWO_{3+x/2} \cdot yH_2O$ nanoplates were obtained using a microwave-assisted hydrothermal methodology, which is cost-effective due to its fast kinetic process. A crystalline tungsten bronze structure was obtained at 150 °C after only 4 min of reaction. H_2O molecules and Na species were detected in the hexagonal channels and improved their electronic properties. The nanoplates exhibited high response as a NO_2 sensor, reaching values higher than 200 and a relatively fast response time (~3 min), showing potential selectivity to NO_2, which involves several applications.

Acknowledgments

FAPESP (2013/07296-2 and 2013/11144-3), CNPq (INCTMN 2008/57872-1 and 573636/2008-7), and CAPES are gratefully acknowledged.

References

[1] V. Hornebecq, J.M. Réau, J. Ravez, Solid State Ion. 127 (2000) 231–240.
[2] R. Brusetti, P. Haen, J. Marcus, Phys. Rev. B 65 (2002) 144528.
[3] T. Gao, B.P. Jelle, J. Phys. Chem. C 117 (2013) 13753–13761.
[4] I. Tsuyumoto, T. Kudo, Sens. Actuators B Chem. 30 (1996) 95–99.
[5] H. Long, W. Zeng, H. Zhang, J. Mater. Sci. Mater. Electron. 26 (2015) 4698–4707.
[6] A.M. El-Sayed, S.M.A. Mousa, Pol. J. Chem. 79 (2005) 1135–1142.
[7] Y.T. Zhu, A. Manthiram, J. Solid State Chem. 110 (1994) 187–189.
[8] A.J. Paula, R. Parra, M.A. Zaghete, J.A. Varela, Mater. Lett. 62 (2008) 2581–2584.
[9] J.F. Fernández-Sánchez, T. Nezel, R. Steiger, U.E. Spichiger-Keller, Sens. Actuat. ors B Chem. 113 (2006) 630–638.
[10] R. Kumar, O. Al-Dossary, G. Kumar, A. Umar, Nano-Micro Lett. 7 (2014) 1–24.
[11] P. Xu, Z. Cheng, Q. Pan, J. Xu, Q. Xiang, W. Yu, et al., Sens. Actuators B Chem. 130 (2008) 802–808.
[12] T. Zhang, J. Su, L. Guo, CrystEngComm 18 (2016) 665–669.
[13] I. Valyukh, Z. Jiao, H. Arwin, X.W. Sun, Thin Solid Films 571 (2014) 644–647.
[14] C. Wang, L. Yin, L. Zhang, D. Xiang, R. Gao, Sensors 10 (2010) 2088–2106.
[15] S. Raj, H. Matsui, S. Souma, T. Sato, T. Takahashi, A. Chakraborty, et al., Phys. Rev. B 75 (2007) 155116.
[16] L. Tolvaj, K. Mitsui, D. Varga, Wood Sci. Technol. 45 (2010) 135–146.
[17] J. Ollitrault, N. Martin, J.Y. Rauch, J.B. Sanchez, F. Berger, Mater. Lett. 155 (2015) 1–3.
[18] Y. He, Z. Wu, L. Fu, C. Li, Y. Miao, L. Cao, et al., Chem. Mater. 15 (2003) 4039–4045.
[19] M.F. Daniel, B. Desbat, J.C. Lassegues, B. Gerand, M. Figlarz, J. Solid State Chem. 67 (1987) 235–247.
[20] B. Miao, W. Zeng, L. Lin, S. Xu, X. Ding, Nanosci. Nanotechnol. Lett. 5 (2013) 765–769.
[21] M. Penza, C. Martucci, G. Cassano, Sens. Actuators B Chem. 50 (1998) 52–59.
[22] C.S. Rout, K. Ganesh, A. Govindaraj, C.N.R. Rao, Appl. Phys. A Mater. Sci. Process. 85 (2006) 241–246.